Role of the extra Fe in $K_{2-x}Fe_{4+y}Se_5$ superconductors

Chih-Han Wang[a,b], Chih-Chien Lee[a], Gwo-Tzong Huang[b], Jie-Yu Yang[b], Ming-Jye Wang[c], Hwo-Shuenn Sheu[d], Jey-Jau Lee[d], and Maw-Kuen Wu[b,1]

[a]Department of Electronic Engineering, National Taiwan University of Science and Technology, Taipei 10607, Taiwan; [b]Institute of Physics, Academia Sinica, Taipei 11529, Taiwan; [c]Institute of Astrophysics and Astronomy, Academia Sinica, Taipei 10617, Taiwan; and [d]Department of Material Science, National Synchrotron Radiation Research Center, Hsinchu 30076, Taiwan

Contributed by Maw-Kuen Wu, November 20, 2018 (sent for review September 5, 2018; reviewed by Robert J. Cava and M. Brian Maple)

The exact superconducting phase of $K_{2-x}Fe_{4+y}Se_5$ has so far not been conclusively decided since its discovery due to its intrinsic multiphase in early material. In an attempt to resolve this mystery, we have carried out systematic structural studies on a set of well-controlled samples with exact chemical stoichiometry $K_{2-x}Fe_{4+x}Se_5$ ($x = 0$–0.3) that are heat-treated at different temperatures. Using high-resolution synchrotron radiation X-ray diffraction, our investigations have determined the superconducting transition by focusing on the detailed temperature evolution of the crystalline phases. Our results show that superconductivity appears only in those samples that have been treated at high-enough temperature and then quenched to room temperature. The volume fraction of superconducting transition strongly depends on the annealing temperature used. The most striking result is the observation of a clear contrast in crystalline phase between the nonsuperconducting parent compound $K_2Fe_4Se_5$ and the superconducting $K_{2-x}Fe_{4+y}Se_5$ samples. The X-ray diffraction patterned can be well indexed to the phase with I4/m symmetry in all temperatures investigated. However, we need two phases with similar I4/m symmetry but different parameters to best fit the data at a temperature below the Fe vacancy order temperature. The results strongly suggest that superconductivity in $K_{2-x}Fe_{4+y}Se_5$ critically depends on the occupation of Fe atoms on the originally empty 4d site.

superconductivity | Fe vacancy disordered | potassium-intercalated iron selenide | intrinsic multiphase

Cuprates and Fe-based high Tc superconductors turn superconducting when their parent compounds are properly doped. The similarity of these superconductors, in which superconductivity emerges with the suppression of competing phases, has created the possibility for a unified picture of high-temperature superconductivity (1, 2). Iron-based superconductors all have FeAs or FeSe layers, just as the CuO_2 layers are the crucial ingredients for superconductivity (3–5). It is generally believed that the quasi-2D characteristics of these active layers and the proximity to magnetically ordered states induce superconductivity via unconventional pairing in these high Tc materials. However, the parent compounds of the Fe-pnictide superconductors are metallic with spin-density wave antiferromagnetic order and with complex underlying electronic structure. This fact, in contrast to the Mott insulators in the cuprates, establishes an important difference between cuprates and pnictides (6, 7).

On the other hand, earlier studies of FeSe superconductor considered this material to be Se deficient (8) so that the exact superconducting stoichiometry was $Fe_{1.01}Se$ (9). Superconductivity in FeSe was found to be closely associated with a structural transition (8, 10, 11), which accompanies a strongly enhanced spin fluctuation near Tc (12). More spectroscopic studies (13–17) suggested modification of the d-orbital-induced pseudogap might be the cause for the structural distortion, which is essential for superconductivity. Later studies indicate that there exists a parent compound (18), which in contrast to having excess Fe is actually Fe deficient and is a Mott insulator. This Fe-deficiency material becomes superconducting after being properly annealed at high temperature (19).

An important development in Fe-based superconductors is the discovery of the relatively higher Tc in alkaline-metal (A) intercalated FeSe with nominal composition $A_{0.8}Fe_2Se_2$ (20). The nominal $A_{0.8}Fe_2Se_2$ sample was considered to crystallize in the tetragonal $ThCr_2Si_2$-type structure, which is isostructural to the $BaFe_2As_2$ system. Researchers have long debated the exact superconducting phase in this material. One group claimed the superconducting composition is identified as $K_{0.83(2)}Fe_{1.64(1)}Se_2$ with enlarged $\sqrt{5} \times \sqrt{5} \times 1$ crystallographic unit cell due to Fe vacancy order (21). The ideal Fe vacancy order phase has a chemical stoichiometry of $K_{0.8}Fe_{1.6}Se_2$ ($K_2Fe_4Se_5$, referred to simply as "245" in the following), which orders antiferromagnetically below 559 K. The second group proposed that the stoichiometric $K_xFe_2Se_2$ phase (which was indexed from X-ray diffraction to exist with about 13% in volume) is the superconducting phase in the matrix of the insulating AF 245 phase (22–24). The third group suggested that superconductivity arises due to the interface between the iron vacancy ordered and free phase (25, 26). Bao et al. (21, 27, 28) have argued that the antiferromagnetic order phase is the origin for superconducting phase, and slightly excess Fe is critical to the stability of the superconducting phase. It was noted that the Fe content of the superconducting samples $K_xFe_{1.6+y}Se_2$ is slightly off-stoichiometry compared with the parent compound 245 (29–33), which seems to play a significant role in the onset of superconductivity.

In our earlier study (34), we identified the ideally Fe vacancy order 245 phase to be a Mott insulator with a block checkerboard

Significance

This paper presents the results of a detailed structural study using synchrotron X-ray diffraction at various temperatures up to 850 °C on $K_{2x}Fe_{4+y}Se_5$ superconductors. The results confirm that extra Fe atoms begin to fill the empty 4d site and stabilize the structural-phase I4/m symmetry so that the lattice size remains the same even above the order–disorder temperature. The results demonstrate that the addition of extra Fe suppresses the Fe vacancy long-range order and the accompanied magnetic order so that superconductivity emerges. The significance of this research is that it provides unambiguously the structural origin for superconductivity in the $K_{2-x}Fe_{4+y}Se_5$ superconducting system.

Author contributions: C.-C.L., M.-J.W., and M.-K.W. designed research; C.-H.W., G.-T.H., and J.-Y.Y. performed research; H.-S.S. and J.-J.L. contributed new reagents/analytic tools; C.-H.W., G.-T.H., M.-J.W., and M.-K.W. analyzed data; and M.-K.W. wrote the paper.

Reviewers: R.J.C., Princeton University; and M.B.M., University of California, San Diego.

The authors declare no conflict of interest.

[1]To whom correspondence should be addressed. Email: mkwu@phys.sinica.edu.tw.

This article contains supporting information online at www.pnas.org/lookup/suppl/doi:10.1073/pnas.1815237116/-/DCSupplemental.

Published online January 7, 2019.

antiferromagnetic (AFM) ordered below 559 K (21, 35). We also reported that superconductivity could be induced with adding small amount of Fe to fill the vacant site plus strong disorder of the Fe vacancy. We noted that the processing temperature has decisive effects on the properties of the samples. Superconducting transition only appears in those samples that have been annealed at high temperature and then quenched. Annealing the superconducting sample at low temperature (<400 °C) gradually suppressed superconductivity. The results showed that superconducting to nonsuperconducting state can switch back and forth in the same sample by changing the heat treatment process. We concluded that the observed facts strongly indicate superconductivity emerges as Fe vacancy becomes disordered.

To understand the effect of annealing conditions to superconductivity better, we carried out a detailed systematic study on a series of samples with stoichiometry $K_{2-x}Fe_{4+y}Se_5$, subject to various annealing temperatures. We also took advantage of the high-resolution X-ray diffraction in the National Synchrotron Radiation Research Center (NSRRC) with in situ high-temperature measurements. Our results revealed that the superconducting volume fraction, even with the same chemical stoichiometry, depends strongly on the annealing (and quench) temperature. There is a critical anneal temperature. Below that temperature, the superconducting volume fraction is close to zero. The results of the high-temperature in situ X-ray diffraction provide further evidence that the random occupation of the original vacant site is the key to superconductivity.

Experimental Procedures

We synthesized polycrystalline bulk samples using an approach described elsewhere in detail (34). DC magnetic susceptibility measurements were performed in a Quantum Design superconducting quantum interference device vibrating sample magnetometer. The synchrotron X-ray diffraction of samples was performed at the BL01C2 BL17A and TPS09A beamline of the NSRRC. The ring of NSRRC was operated at energy 1.5 GeV with a typical current of 360 mA. The wavelengths of the incident X-rays were 0.61993, 1.3216, and 0.77491 Å, delivered from the 5-T Superconducting Wavelength Shifter and a Si(111) triangular crystal monochromator. Two pairs of slits and one collimator were set up inside the experimental hutch to provide a collimated beam with dimensions of typical 0.5 mm × 0.5 mm (horizontal × vertical) at the sample position. The diffraction pattern was recorded with a Mar345 imaging plate detector ~400 mm from the sample, with a typical exposure duration of 1 min. The pixel size of Mar345 was 100 m. The 1D powder diffraction profile was converted with program GSAS II and cake-type integration. The diffraction angles were calibrated according to Bragg positions of LaB6 standards.

Results and Discussion

Fig. 1*A* shows the X-ray diffraction pattern of three $K_{2-x}Fe_{4+x}Se_5$ samples with x ranging from 0.1 to 0.2. The *Inset* displays the relevant magnetic susceptibility of the samples. The magnetic data indicate that the superconducting diamagnetic signal diminishes with reducing K content, with almost no diamagnetic signal in $K_{1.8}Fe_{4.2}Se_5$. Meanwhile the X-ray diffraction patterns show no additional peaks, which have been associated with the extra $K_zFe_2Se_2$ phase by other groups (22), in this nonsuperconducting $K_{1.8}Fe_{4.2}Se_5$ sample. Based on this observation, one would consider that superconductivity might originate from this extra $K_zFe_2Se_2$ phase. However, close examination of the X-ray and magnetic data of two $K_{1.9}Fe_{4.2}Se_5$ samples, as shown in Fig. 1*B*, which are prepared under different annealing and quenching temperatures, one at 650 °C and the other at 790 °C, shows a high-volume superconducting signal in the sample prepared at 790 °C, but no diamagnetic signal in sample prepared at 650 °C. The X-ray diffraction patterns for both samples are almost identical, showing the presence of the extra peaks associated with $K_zFe_2Se_2$ phase. The above contradictory observations suggest that there are more subtleties regarding the correlation between crystal structure and superconductivity in this intriguing superconducting system.

Subsequently, we carried out detailed X-ray diffractions at different temperatures up to 750 °C for the $K_2Fe_4Se_5$ (2(4)5) and excess-Fe $K_{1.9}Fe_{4.2}Se_5$ (1.9(4.2)5) samples. Both the warming and cooling cycles exhibit no difference in the diffraction patterns, as shown in Fig. 2. Fig. 2*A* illustrates the significant shifts in diffraction peaks (008) and (051) at 275 °C in warming, which are the indication of the transition from the Fe vacancy order to disorder state. A large hysteresis shows the transition temperature was reduced to 240 °C in cooling cycle. Below the transition temperature, the material exhibits clearly the Fe vacancy order of I4/m symmetry with $\sqrt{5} \times \sqrt{5}$ superlattice; and above the order temperature, the crystal symmetry seems to fit well to I4/mmm symmetry. In addition, the superstructural peaks related to the vacancy order state completely disappear above the ordering temperature. However, since the chemical stoichiometry of the

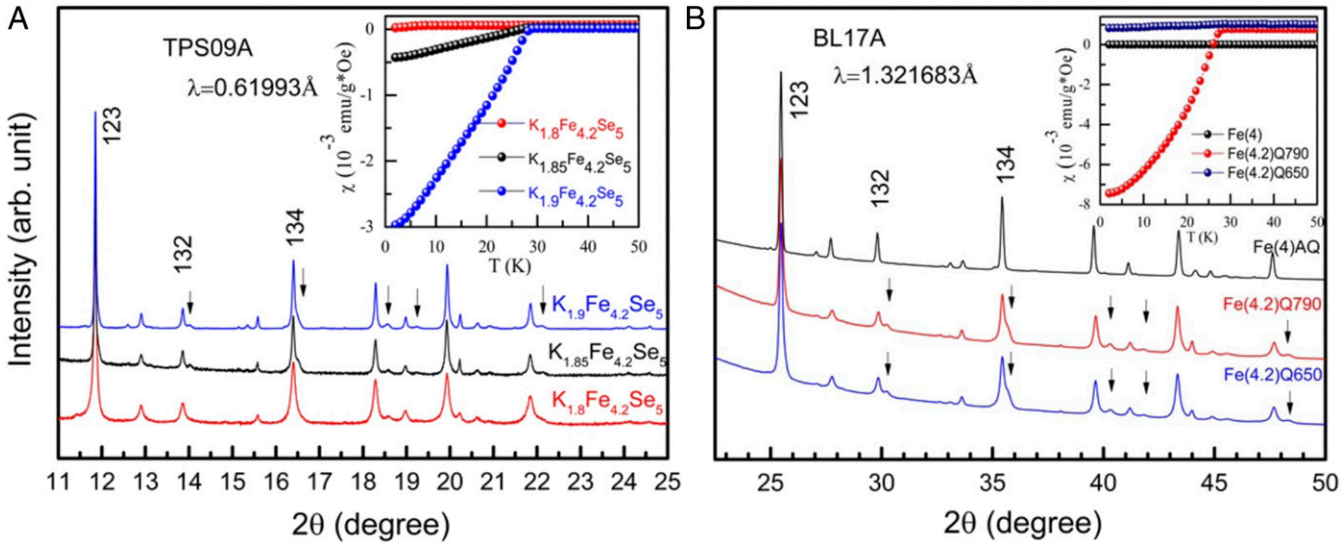

Fig. 1. X-ray diffraction patterns of polycrystalline $K_{2-x}Fe_{4+y}Se_5$ samples. (*A*) $K_{2-x}Fe_{4.2}Se_5$ quenched from 820 °C. The marks point out the second phase. When K content decreases, the second phase gradually disappears. (*B*) $K_{1.9}Fe_{4.2}Se_5$ quenched in 650 °C and 790 °C. The same composition with the same structure shows no superconductivity quenched from 650 °C. The *Inset* is the magnetic susceptibility measured in a 30 Oe field under zero-field–cooled (ZFC) conditions.

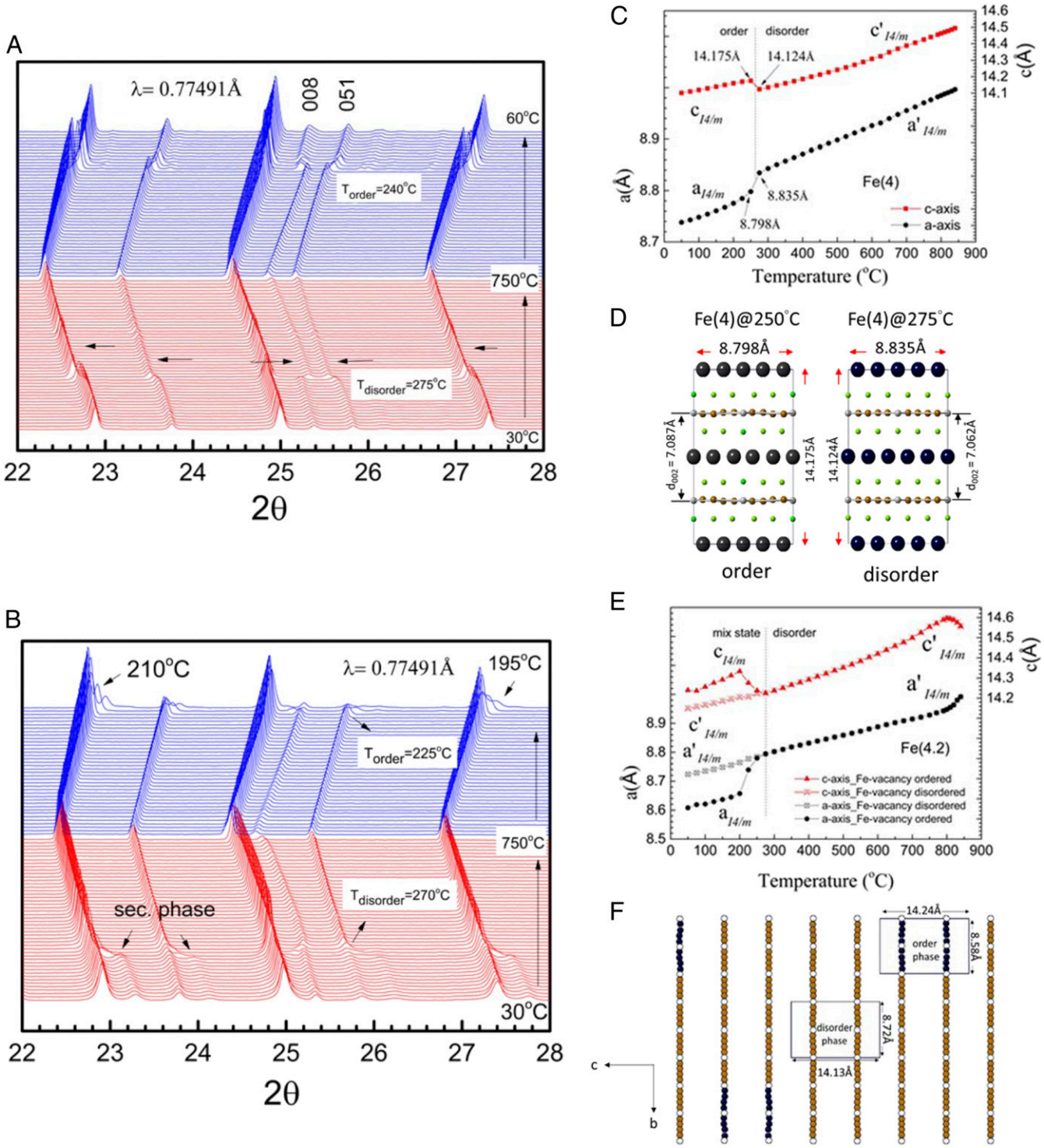

Fig. 2. Evolution of the temperature-dependent X-ray powder diffraction pattern of (*A*) $K_2Fe_4Se_5$ (245) and (*B*) $K_{1.9}Fe_{4.2}Se_5$ (2(4.2)5). The color red indicates increasing temperature; blue indicates decreasing temperature. Refined lattice parameters of $K_2Fe_4Se_5$ and $K_{1.9}Fe_{4.2}Se_5$ samples are displayed in *C* and *E*, respectively. All data are refined using the I4/m unit cell. A cell with compressed *c* axis and expanded *ab* plane is observed above vacancy disorder temperature in 245 sample; two cells with different lattice parameters (one for vacancy-ordered cell and the other for vacancy-disordered) are found to best fit the data for 2(4.2)5 sample below Fe vacancy disorder temperature. *D* illustrates the I4/m unit cell. The *Left* cell is Fe vacancy-ordered phase, and the *Right* cell is disordered phase. In the Fe vacancy order phase, the mirror image of Fe2 (16i) layers is according to magnetic moment orientation (21). The disordered phase shows that the *c* axis is compressed, and *ab* plane is expanded. *F* shows the schematic of mix structure, which includes both ordered and disordered phases. The black boxes outline the I4/m unit cell. The iron vacancy site (4d) is marked by the hollow symbol, and the Fe(16i) site is marked by the khaki (black) color. K and Se atoms are not shown in the plot.

Table 1. The structural information for $K_2Fe_4Se_5$ (275 °C) as Rietveld refinement from the synchrotron diffraction data

Space group: I4/m						Space group: I4/mmm					
a (Å) = 8.834865		c (Å) = 14.123927		$\alpha = \beta = \gamma = 90°$		a (Å) = 3.951249		c (Å) = 14.124636		$\alpha = \beta = \gamma = 90°$	
	x	y	z	Mult.	Occ.		x	y	z	Mult.	Occ.
K_1 (2b)	0	0	0.5	2	0.9206	K_1 (2b)	0	0	0	2	0.8044
K_2 (8h)	0.797342	0.403553	0.5	8	0.7817	Fe_1 (4d)	0	0.5	0.25	4	0.7980
Fe_1 (4d)	0	0.5	0.25	4	0.7989	Se_1 (4e)	0	0	0.354242	4	1.0017
Fe_2 (16i)	0.300480	0.396745	0.249143	16	0.8022						
Se_1 (4e)	0	0	0.147326	4	1.0709						
Se_2 (16i)	0.100799	0.299760	0.354629	16	0.9896						

Rwp = 5.40%, Rp = 3.93%, x^2 = 0.09295. Rwp = 5.47%, Rp = 4.01%, x^2 = 0.09351.

sample was exactly 245, it was a puzzle to us: how could the high-temperature phase belong to the high-symmetry I4/mmm group as there is 20% Fe deficiency? Thus, we tried to fit the diffraction pattern with I4/m symmetry considering that the high-temperature phase Fe could occupy both 16i (fully occupied) and 4d site (originally empty site). The fitting was almost perfect and the resulted lattice parameters are shown in Table 1, which is almost identical to those values obtained by fitting with I4/mmm. This result indicates the crystal structure of 245 could be well described by single phase with I4/m symmetry even above 285 °C (28).

We were surprised when we first saw the temperature-dependent diffraction patterns of the excess-Fe sample that exhibits bulk superconductivity, as shown in Fig. 2*B*, which show essentially no shift in all diffraction peak positions throughout the whole temperature range. We carefully examined the diffraction patterns, as shown in Figs. 2*B* and 3, and we found additional peaks below the vacancy-order temperature at 270 °C during warming. The data for 2(4.2)5 sample are found to best fit with two different sets of parameters (shown in Table 2), one with Fe vacancy ordered and the other disordered Fe vacancy, under the same I4/m symmetry. Fig. 2 *C* and *E*) plot the lattice parameters of 245 and 2(4.2)5 samples, respectively, below (both fit with I4/m symmetry) and above the Fe vacancy order temperature. Fig. 2 *D* and *F* are the schematic atomic arrangements for the two samples based on the refined results.

Fig. 3 *A* and *B* displays the diffraction patterns for 245 and 2(4.2)5 samples plotting with diffraction angles and d spacing, respectively. There are two phases coexisting in excess-Fe sample shown in Fig. 3*A*. The *Inset* shows the superlattice (110) profile. The intensity of diffraction peak in the excess-Fe sample is not only decreased but also shifted to a higher angle. It suggests the Fe vacancy ordered phase of the excess-Fe sample, which has *a*-axis parameters significantly smaller than 245. From Fig. 3*B*, those additional features can be associated with the Miller index (002), (130), (132), (134), (136) … Fe-layers, based on I4/m symmetry. Fig. 3*C* shows the schematic atomic arrangement of the plane (132) in the vacancy ordered and disordered states. The d spacing for the disordered state is about 2% larger than that of the ordered state. These planes are all crossing the Fe-4d site, as exemplified by the schematic plot in Fig. 3*D*. This result indicates that the presence of excess-Fe atoms shall begin to fill the original empty 4d sites (construct the disorder phase). Thus, additional planes with the same Miller index show up. Our analysis shows that the difference in d-spacing of these new features with the original peaks is at most 2%, as displayed in Fig. 3*B*. These additional features disappear above the vacancy order–disorder transition temperature, but keep the diffraction peak positions unchanged. This observation suggests that the added excess-Fe atoms play a critical role in maintaining the crystal lattice (high temperature phase) with the I4/m symmetry as that of the vacancy ordered state. Above the vacancy order temperature, the lattice remains with the I4/m symmetry but with disorder occupation of the Fe-atom to all possible Fe site so that the additional features disappear.

It is known that for tetragonal symmetry the peak of (hkl) and (khl) are at the same diffraction angle because $a = b$, whereas for orthorhombic symmetry the peak of (hkl) and (hkl) could be at different diffraction angle because $a \neq b$. Thus, we have also tried to fit the observed diffraction patterns by considering whether the data fit with orthorhombic symmetry. Detailed analysis of the data suggests that a monoclinic 245 structure with I112/m symmetry, using the lattice parameters: a = 8.6 Å, b = 8.72 Å, c = 14.2 Å, and γ = 90°, could generate most of the diffraction peaks observed (as shown in *SI Appendix*). Although the diffraction peaks seem to fit well with the observed results, the overall refinement was relatively poor regarding the peak intensity, which is known to depend on the number, position, and specie of atoms.

Table 2. The structural information for $K_{1.9}Fe_{4.2}Se_5$ (25 °C) as Rietveld refinement from the synchrotron diffraction data

Fe vacancy disorder phase (86.3%)						Fe vacancy order phase (13.7%)					
a (Å) = 8.717743		c (Å) = 14.1251740		$\alpha = \beta = \gamma = 90°$		a (Å) = 8.582171		c (Å) = 14.235626		$\alpha = \beta = \gamma = 90°$	
	x	y	z	Mult.	Occ.		x	y	z	Mult.	Occ.
K_1 (2b)	0	0	0.5	2	0.8509	K_1 (2b)	0	0	0.5	2	0.7841
K_2 (8h)	0.808077	0.392152	0.5	8	0.8074	K_2 (8h)	0.732769	0.398093	0.5	8	0.6877
Fe_1 (4d)	0	0.5	0.25	4	0.2214	Fe_1 (4d)	0	0.5	0.25	4	0.0000
Fe_2 (16i)	0.295179	0.406466	0.250104	16	1.0083	Fe_2 (16i)	0.293777	0.403941	0.252191	16	1.0315
Se_1 (4e)	0	0	0.137406	4	1.0006	Se_1 (4e)	0	0	0.144785	4	1.0324
Se_2 (16i)	0.110745	0.292429	0.353529	16	0.9878	Se_2 (16i)	0.101194	0.302082	0.357016	16	0.9602

Rwp = 2.94%, Rp = 2.19%, χ^2= 0.05283. Space group: I4/m.

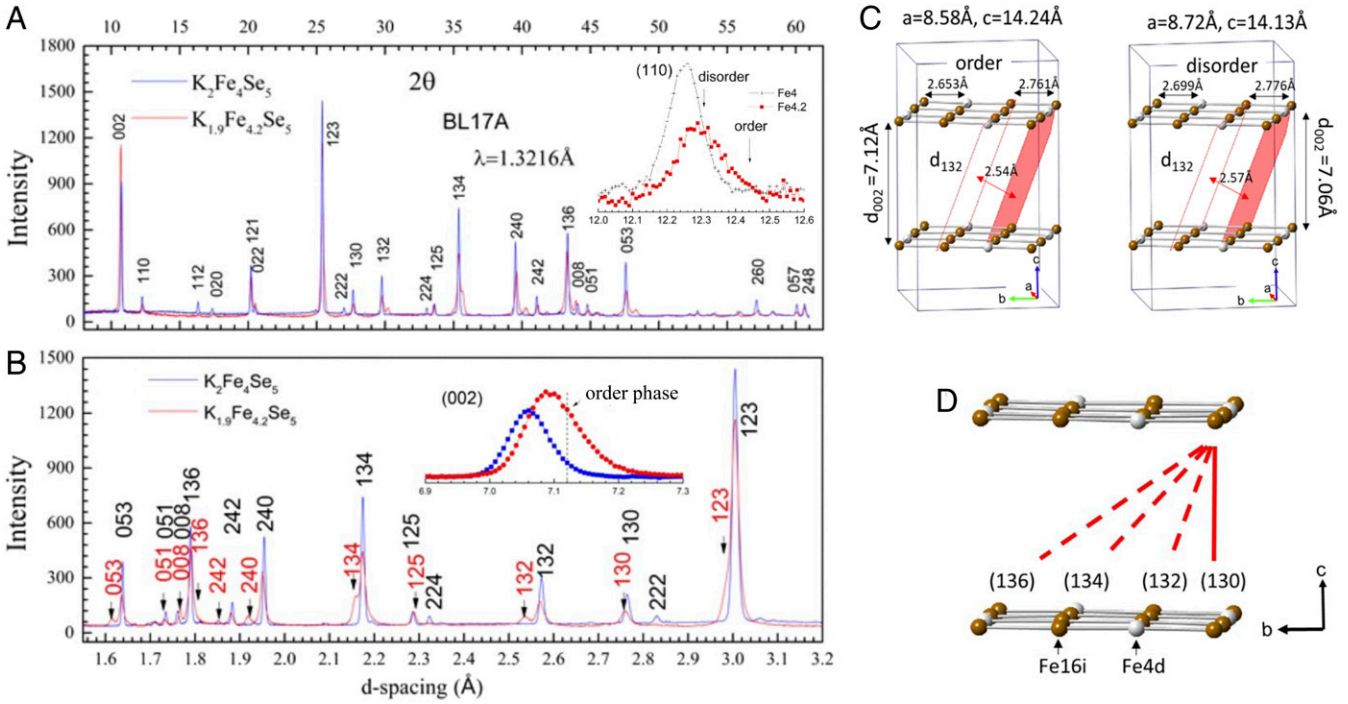

Fig. 3. Synchrotron powder diffraction patterns of the polycrystalline $K_{2-x}Fe_{4+y}Se_5$ samples. (*A*) Superconducting 1.9(4.2)5 and nonsuperconducting parent 245 X-ray diffraction pattern in diffraction angles. The superlattice peaks, for example, (222) and (224) peaks, are almost suppressed in the superconducting 1.9(4.2)5 sample. *Inset* shows the (110) diffraction profile. (*B*) The same diffraction patterns displayed with lattice d spacing show that there are two similar phases in 1.9(4.2)5 sample. One is similar to 245 parent phase but without (222) superlattice, and the other with slightly smaller d spacing analyzed. *Inset* shows the (002) profile. (*C*) Illustration of the two similar phases with difference in d spacing for (132) plane. (*D*) Schematic of (130), (132), (134), and (136) plane. The iron vacancy site 4d is marked by the white symbol, and the 16i site is marked with khaki color.

Based on the above observations, one might expect even in the stoichiometry 245 sample to observe that Fe atoms occupied the empty 4d site if the sample has been treated at high-enough temperature so that Fe atoms could hop around. Indeed, the high-resolution X-ray diffraction patterns of the 245 sample quenched from 800 °C, as shown in Fig. 4, display extra peaks similar to those observed in excess-Fe samples. Meanwhile, the magnetic susceptibility data shown in the *Inset* of Fig. 4 exhibits clearly diamagnetic signal indicating the presence of superconductivity, although its volume fraction is rather small. These results demonstrate that the occupation of the 4d site, which maintains the crystal lattice (size), plays a key role for the emergence of superconductivity. It is noted that there is a significant temperature hysteresis in the vacancy order–disorder transition as on cooling the additional features do not appear until below 240 °C, suggesting this transition is first-order thermodynamically.

To clarify further the role of the extra Fe atom to the crystal lattice, two more samples were prepared for detailed studies: $K_{1.9}Fe_{4.05}Se_5$ and $K_{1.9}Fe_{4.25}Se_5$. As shown in Fig. 5, the changes in diffraction peak positions of (0 0 8) and (0 5 1) for the $K_{1.9}Fe_{4.05}Se_5$ sample clearly are less significant compared with that of the 245 sample. For the $K_{1.9}Fe_{4.25}Se_5$ sample, essentially the same as the $K_{1.9}Fe_{4.2}Se_5$ sample, the peak positions do not change with temperature. These results further confirm that extra-Fe atoms begin to fill the empty 4d site and stabilize the structural phase I4/m symmetry so that the lattice size remains the same above the order–disorder temperature. By comparing with the parent compound, the extra-Fe sample exhibits much weaker superstructural peaks such as the (222) peak, which almost disappears at room temperature. This demonstrates that the addition of extra Fe suppresses the Fe vacancy long-range order. Consequently, this modification suppresses the magnetic order, which accompanies with the vacancy order, to favor the emergence of superconductivity.

Our experimental observations further confirm that superconductivity in $K_{2-x}Fe_{4+y}Se_5$ is not due to the impurity phase ($K_{0.5}Fe_2Se_2$), which has been suggested based on the X-ray diffraction features. Our results unambiguously demonstrate that the random occupation of Fe atom in the lattice is key for superconductivity. Nevertheless, the exact origin for superconductivity

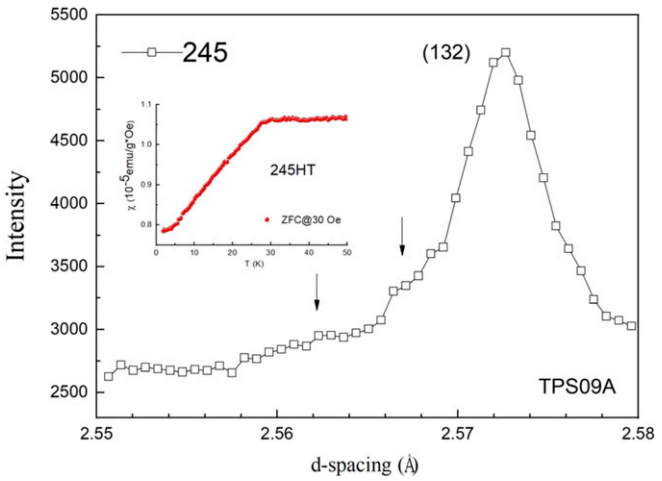

Fig. 4. Synchrotron powder diffraction patterns of the polycrystalline 245HT sample. Diffraction profile of the (132) plane is shown. The multiphase profile of 245HT is similar to those observed in excess Fe samples. *Inset* displays a clear diamagnetic signal at 29.6 K. *Inset* reproduced with permission from ref. 34.

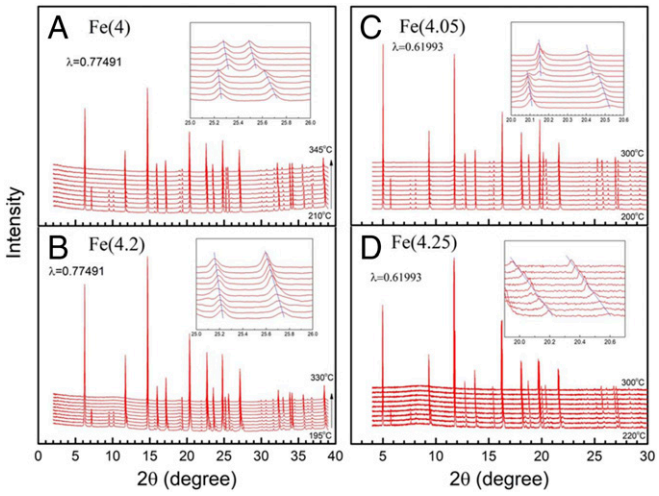

Fig. 5. Temperature-dependent in situ X-ray powder diffraction pattern of (*A*) $K_2Fe_4Se_5$, (*B*) $K_{1.9}Fe_{4.2}Se_5$, (*C*) $K_{1.9}Fe_{4.05}Se_5$, and (*D*) $K_{1.9}Fe_{4.25}Se_5$. The *Inset* enlarges 2θ within the range 25° < 2θ < 26° and 20° < 2θ < 21° (depending on wavelength λ). The pictures show that when temperature is higher than Ts (*A*) Fe(4) lattice constant has obvious change, (*C*) Fe(4.05) lattice constant has minor change, and (*B*) Fe(4.2) and (*D*) Fe(4.25) are almost the same. This indicates excess Fe stabilizes the 245 structure.

remains to be resolved. Several questions remain to be answered, such as, why does the superconducting volume fraction in the excess-Fe sample depend on the annealing and quenching temperature? We are currently working on a detailed refinement of the X-ray diffraction data, collected with a wide temperature range. A preliminary result indicates that a more subtle high-temperature structural distortion might be closely related to the appearance of superconductivity. Details of these results will be published in the near future.

Summary

In summary, in this detailed X-ray diffraction experiment over a wide range of temperature, we have showed that the superconducting $K_{2-x}Fe_{4+y}Se_5$ samples with excess Fe atoms exhibit the same structure with I4/m symmetry throughout the whole temperature range studied. The observation of extra features, which have been considered by others as the presence of impurity phase associated with the I4/mmm symmetry, actually were the signatures of the original empty Fe-4d sites occupied by the excess Fe atoms. The occupation of the Fe-4d site and an eventual more random distribution of the Fe atom are critical to the emergence of superconductivity. Therefore, the main conclusion of this study further confirms that superconductivity in $K_{2-x}Fe_{4+y}Se_5$, very much similar to that observed in high Tc cuprates, is derived from the doping (adding extra Fe) to the parent Mott insulator $K_2Fe_4Se_5$. More disorder of the Fe occupation in the I4/m lattice leads to higher volume fraction of superconductivity. We are investigating a more detailed refinement of the high-temperature diffraction data to unravel the exact origin for the appearance of superconductivity in this intriguing FeSe-based superconductor.

ACKNOWLEDGMENTS. We thank Chung-Kai Chang for fruitful discussion and valuable suggestions in synchrotron powder X-ray diffraction measurement. We appreciate the help from Drs. Phillip Wu, Michelle Kuo, and Albert Wu in preparing this manuscript. This research is supported by Ministry of Science and Technology Grant MOST106-2633M-001-001, Academia Sinica Thematic Research Grant AS-TP-106-M01, and the National Synchrotron Radiation Research Center, Taiwan.

1. Johnston DC (2010) The puzzle of high temperature superconductivity in layered iron pnictides and chalcogenides. *Adv Phys* 59:803–1061.
2. Paglione J, Greene RL (2010) High-temperature superconductivity in iron-based materials. *Nat Phys* 6:645–658.
3. Dagotto E (1994) Correlated electrons in high-temperature superconductors. *Rev Mod Phys* 66:763–840.
4. Scalapino DJ (1995) The case for dx2 − y2 pairing in the cuprate superconductors. *Phys Rep* 250:329–365.
5. Dagotto E (2013) Colloquium: The unexpected properties of alkali metal iron selenide superconductors. *Rev Mod Phys* 85:849–867.
6. Hirschfeld PJ, Korshunov MM, Mazin II (2011) Gap symmetry and structure of Fe-based superconductors. *Rep Prog Phys* 74:124508.
7. Stewart GR (2011) Superconductivity in iron compounds. *Rev Mod Phys* 83:1589.
8. Hsu FC, et al. (2008) Superconductivity in the PbO-type structure alpha-FeSe. *Proc Natl Acad Sci USA* 105:14262–14264.
9. McQueen TM, et al. (2009) Extreme sensitivity of superconductivity to stoichiometry in $Fe_{1+\delta}Se$. *Phys Rev B Condens Matter Mater Phys* 79:014522.
10. Wang MJ, et al. (2009) Crystal orientation and thickness dependence of the superconducting transition temperature of tetragonal $FeSe_{1-x}$ thin films. *Phys Rev Lett* 103:117002.
11. McQueen TM, et al. (2009) Tetragonal-to-orthorhombic structural phase transition at 90 K in the superconductor $Fe_{(1.01)}Se$. *Phys Rev Lett* 103:057002.
12. Imai T, Ahilan K, Ning FL, McQueen TM, Cava RJ (2009) Why does undoped FeSe become a high-Tc superconductor under pressure? *Phys Rev Lett* 102:177005.
13. Wen Y-C, et al. (2012) Gap opening and orbital modification of superconducting FeSe above the structural distortion. *Phys Rev Lett* 108:267002.
14. Zhang AM, et al. (2012) Two-magnon Raman scattering in $A_{0.8}Fe_{1.6}Se_2$ systems (A = K, Rb, Cs, and Tl): Competition between superconductivity and antiferromagnetic order. *Phys Rev B Condens Matter Mater Phys* 85:214508.
15. Zhang AM, et al. (2012) Effect of iron content and potassium substitution in A0.8Fe1.6Se2 (A=K, Rb, Tl) superconductors: A Raman scattering investigation. *Phys Rev B Condens Matter Mater Phys* 86:134502.
16. Yi M, et al. (2013) Observation of temperature-induced crossover to an orbital-selective Mott phase in A(x)Fe(2-y)Se2 (A=K, Rb) superconductors. *Phys Rev Lett* 110:067003.
17. Maletz J, et al. (2014) Unusual band renormalization in the simplest iron-based superconductor FeSe1_x. *Phys Rev B* 89:220506.
18. Chen TK, et al. (2014) Fe-vacancy order and superconductivity in tetragonal β-Fe1-xSe. *Proc Natl Acad Sci USA* 111:63–68.
19. Chang C-C, et al. (2012) Superconductivity in PbO-type tetragonal FeSe nanoparticles. *Solid State Commun* 152:649–652.
20. Guo J, et al. (2010) Superconductivity in the iron selenide KxFe2Se2 ($0 \le x \le 1.0$). *Phys Rev B* 82:180520.
21. Bao W, et al. (2011) A novel large moment antiferromagnetic order in $K_{0.8}Fe_{1.6}Se_2$ superconductor. *Chin Phys Lett* 28:086104.
22. Carr SV, et al. (2014) Structure and composition of the superconducting phase in alkali iron selenide $K_yFe_{1.6+x}Se_2$. *Phys Rev B Condens Matter Mater Phys* 89:134509.
23. Shoemaker DP, et al. (2012) Phase relations in $K_xFe_{2-y}Se_2$ and the structure of superconducting $K_xFe_2Se_2$ via high-resolution synchrotron diffraction. *Phys Rev B Condens Matter Mater Phys* 86:184511.
24. Wang Z, et al. (2015) Archimedean solidlike superconducting framework in phase-separated $K_{0.8}Fe_{1.6+x}Se_2$ (0≦x≦0.15). *Phys Rev B Condens Matter Mater Phys* 91:064513.
25. Li W, et al. (2012) KFe_2Se_2 is the parent compound of K-doped iron selenide superconductors. *Phys Rev Lett* 109:057003.
26. Duan C, et al. (2018) Appearance of superconductivity at the vacancy order-disorder boundary in $K_xFe_{2-y}Se_2$. *Rev B* 97:184520.
27. Ye F, et al. (2011) Common crystalline and magnetic structure of superconducting $A_2Fe_4Se_5$ (A=K,Rb,Cs,Tl) single crystals measured using neutron diffraction. *Phys Rev Lett* 107:137003.
28. Bao W (2015) Structure, magnetic order and excitations in the 245 family of Fe-based superconductors. *J Phys Condens Matter* 27:023201.
29. Wang Z-W, et al. (2012) Structural phase separation in $K_{0.8}Fe_{1.6+x}Se_2$ superconductors. *J Phys Chem C* 116:17847.
30. Peng F, Liu WP, Lin CT (2013) Study of thermal behavior and single crystal growth of $A_{0.8}Fe_{1.81}Se_2$ (A = K, Rb, and Cs). *J Supercond Nov Magn* 26:1205–1211.
31. Liu Y, et al. (2016) Formation mechanism of superconducting phase and its three-dimensional architecture in pseudo-single-crystal $K_xFe_{2-y}Se_2$. *Phys Rev B* 93:064509.
32. Yang J, et al. (2016) Strong correlations between vacancy and magnetic ordering in superconducting K0.8Fe2_ySe2. *Phys Rev B* 94:024503.
33. Ricci A, et al. (2011) Nanoscale phase separation in the iron chalcogenide superconductor $K_{0.8}Fe_{1.6}Se_2$ as seen via scanning nanofocused x-ray diffraction. *Phys Rev B* 84:060511.
34. Wang C-H, et al. (2015) Disordered Fe vacancies and superconductivity in potassium-intercalated iron selenide ($K_{2-x}Fe_{4+y}Se_5$). *Europhys Lett* 111:27004.
35. Wei B (2013) Physics picture from neutron scattering study on Fe-base superconductors. *Chin Phys B* 22:087405.